LFM ISAR Signal Model and Image Reconstruction

Andon Dimitrov Lazarov
Bourgas Free University, 62 San Stefano Str., 8000 Bourgas, Bulgaria
Tel: +35956900485, Fax: +35956900515,
lazarov@bfu.bg

ABSTRACT

In the present work a new model of the Inverse Synthetic Aperture Radar (ISAR) Linear Frequency Modulated (LFM) signal as a geometrical sum of emissions of point scatterers from the object space is addressed. It describes the amplitude and phase of the ISAR signal reflected from a target with a complicated shape. The geometry of the target is depicted by reference points in three-dimensional (3-D) coordinate system. Basic analytical geometrical and kinematical equations are derived. The model allows describing variety of kinematical states of the target. New definition of the discrete fast time parameter as a function of the number of radar range resolution cells is proposed. Description and graph illustration of the process of the LFM ISAR signal formation is presented. All stages of the image reconstruction, including demodulation, range alignment, range compression, azimuth compression and autofocusing are mathematically defined. Entropy as a cost function is used to implement iterative image quality enhancement. Numerical experiment to verify the ISAR geometry; signal model and image reconstruction algorithm is carried out.

1. INTRODUCTION

The inverse synthetic aperture radar (ISAR) technique is an efficient and well-know approach to obtain high quality images of moving objects [1-4]. This method consists in coherent processing of ISAR signal returns, reflected from the object and obtained during its relative motion with respect to the ISAR system, placed in the origin of the coordinate system of observation. High range resolution of the image can be achieved transmitting to the object signals with a large bandwidth. High azimuth resolution can be realized using large synthetic aperture length.

A classical image reconstruction technique in the ISAR theory is a focusing correlation procedure over the coherent detected ISAR signal and reference function, the signal reflected by a point scatterer with completely known kinematical parameters. In order to avoid the necessity of a reference function and apply a standard FFT signal processor a special phase correction, called autofocusing has to be used [5-10]. It can be interpreted as a motion compensation of higher order and requires determination of higher order terms of the Tailor expansion of the reference function. From physical point of view each movement of the object can be divided into radial displacement of its mass/geometrical center on the line of sight and rotation of the object over the mass center. Simple mathematical image reconstruction expressions can be derived while considering only rotational motion of the object around its mass centre [2, 3, 5, and 10]. In this case the first step of the image reconstruction is the compensation of the radial displacement of the object's mass centre, if it can be measured precisely. It allows exploiting powerful image reconstruction computational instruments as parametric and semi-parametric methods of Peter Stoica [11-15]. In this work without resorting to the concept of dividing of the object movement into radial and rotational one, rectilinear movement of the object will be considered based on the fact that the speed of the object of interest is very high and the time of observation is too short (around 0.5-1 s). Recently the models used to describe ISAR signals are thoroughly two-dimensional (2-D) one [1-15]. 3-D image reconstruction algorithms have been created using different mathematical description of ISAR signal models [16-18]. Few authors consider a 3-D geometry of the ISAR scenario without description of the 3-D geometry of the object and its multiple positions in the 3-D space. Therefore in the present work an ISAR signal model which depends on three geometrical coordinates of the object and its space orientation is proposed. In that

aspect the outcomes in this work pretend to fill in the gap in the ISAR analysis.

The LFM signals possess acceptable range resolution capability and therefore widely used in the ISAR practice. Hence, the 3-D ISAR scenario description, all stages of image reconstruction procedure including range alignment, range and azimuth compression and phase correction with application of LFM emitted signals are of particular interest. Accordingly, the main goal of the present work is analytically to describe the 3-D geometry of ISAR scenario, deterministic components of the LFM ISAR signal reflected from objects with complicated shape, and image reconstruction algorithms with autofocusing capabilities.

The remainder of the paper is organized as follows. In section II an analytical description of the 3-D ISAR geometry is given. In Section III the LFM ISAR pulses and model of deterministic components of the ISAR signal are described. In Section IV an image reconstruction and phase correction algorithm based on entropy minimization is presented. In Section V results of a numerical experiment are given. In Section VI conclusions of the current investigation are made.

2. GEOMETRY OF ISAR SCENARIO

It is assumed that the object is detected in a 3-D regular grid defined in a Cartesian system $O'XYZ$ [19] and described by reference points placed at each node of the 3-D grid (Fig. 1). The object is moving in a coordinate system $Oxyz$ on a rectilinear trajectory with a constant velocity V. The mass-center of the object, the geometrical center of the 3-D grid and the origin of the coordinate system $O'XYZ$ coincide. The range vector, $\mathbf{R}_{ijk}(p)=\left[x_{ijk}(p), y_{ijk}(p), z_{ijk}(p)\right]^T$ from the ISAR placed in the origin of the coordinate system $Oxyz$ to the ijkth point scatterer from the object space, is defined by the vector equation

$$\mathbf{R}_{ijk}(p)=\mathbf{R}_{00}(0)+\mathbf{V}T_p\left(\frac{N}{2}-p\right)+\mathbf{A}\mathbf{R}_{ijk} \tag{1}$$

where $\mathbf{R}_{00}(0)=\left[x_{00}(0), y_{00}(0), z_{00}(0)\right]^T$ is the line-of-sight vector to the geometrical center of the object at the discrete moment $p=N/2$, T_p is the pulse repetition period (the measure of the slow time parameter), $p=\overline{0,\ N-1}$ is the current number of emitted pulse and N is the full number of emitted pulses, $\mathbf{V}=\left[V\cos\alpha, V\cos\beta, V\cos\delta\right]^T$ is the vector velocity, $\mathbf{R}_{ijk}=\left[X_{ijk}, Y_{ijk}, Z_{ijk}\right]^T$ is the distance vector to the ijkth reference point in the coordinate system $O'XYZ$; $(.)^T$ is the transposition; $X_{ijk}=i(\Delta X)$, $Y_{ijk}=j(\Delta Y)$ and $Z_{ijk}=k(\Delta Z)$ are the discrete coordinates of the ijkth reference point in the coordinate system $O'XYZ$; ΔX, ΔY and ΔZ are the spatial dimensions of the 3-D grid's cell; $\cos\alpha$, $\cos\beta$ and $\cos\delta=\sqrt{1-\cos^2\alpha-\cos^2\beta}$ are the guiding cosines, and V is the modulus of the vector velocity $\mathbf{V}$.

The geometry of the 3-D ISAR scenario is described in Fig. 1. The point O' with coordinates $x_{00}(0), y_{00}(0), z_{00}(0)$ at the moment $p=N/2$ is the origin of the coordinate system $O'XYZ$. The point $R(0)$ with coordinates $x_0(0), y_0(0), z_0(0)$ is located in a reference plane, which determines the position of the object in the space.

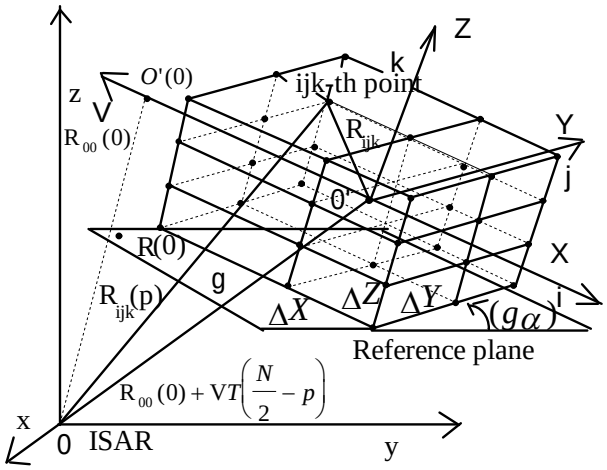

Figure: 1. ISAR Geometry

The elements of the transformation matrix **A** in equation (1) are described by the following Euler expressions

$$
\begin{aligned}
a_{11} &= \cos\psi\cos\varphi - \sin\psi\cos\theta\sin\varphi;\\
a_{12} &= -\cos\psi\sin\varphi - \sin\psi\cos\theta\cos\varphi;\\
a_{13} &= \sin\psi\sin\theta;\\
a_{21} &= \sin\psi\cos\varphi + \cos\psi\cos\theta\sin\varphi;\\
a_{31} &= \sin\theta\sin\varphi;\\
a_{22} &= -\sin\psi\sin\varphi + \cos\psi\cos\theta\cos\varphi;\\
a_{32} &= \sin\theta\cos\varphi;\\
a_{23} &= -\cos\psi\sin\theta;\quad a_{33} = \cos\theta.
\end{aligned}
\tag{2}
$$

The space angles ψ, θ and φ can be interpreted as a yaw, pitch and roll angles and calculated by components A,B,C of the normal vector to the plane, where the trajectory of the object mass-center lies, and coordinates of the vector velocity, i.e.

$$
\psi = \arctan\left(-\frac{A}{B}\right); \qquad \theta = \arccos\frac{C}{[(A)^2 + (B)^2 + (C)^2]^{\frac{1}{2}}}, \tag{3}
$$

$$
\varphi = \arccos\frac{V_x B - V_y A}{\{[(A)^2 + (B)^2][(V_x)^2 + (V_y)^2 + (V_z)^2]\}^{\frac{1}{2}}}. \tag{4}
$$

The components A,B,C of the normal vector are calculated by the coordinates A^0, B^0, C^0 of the normal vector to a preliminary known oriented reference plane g in the space, the coordinates of the vector velocity and the angle $(g\alpha)$ between the trajectory plane and the reference plane, i.e.

$$
A = \frac{A^0.V.\cot(g\alpha) + C^0 V_y - B^0 V_z}{(A^0)^2 + (B^0)^2 + (C^0)^2} \tag{5}
$$

(6) $$B = \frac{B^0.V.\cot(g\alpha) + A^0V_z - C^0V_x}{(A^0)^2 + (B^0)^2 + (C^0)^2}$$

(7) $$C = \frac{C^0.V.\cot(g\alpha) + B^0V_x - A^0V_y}{(A^0)^2 + (B^0)^2 + (C^0)^2}$$

where A^0, B^0 and C^0 are the components of the normal vector to the plane g and defined by the expressions

(8) $$\begin{aligned} A^0 &= V_z[y_{00}(0) - y_0(0)] - V_y[z_{00}(0) - z_0(0)]; \\ B^0 &= V_x[z_{00}(0) - z_0(0)] - V_z[x_{00}(0) - x_0(0)]; \\ C^0 &= V_y[x_{00}(0) - x_0(0)] - V_x[y_{00}(0) - y_0(0)], \end{aligned}$$

If the angle $(g\alpha)$ is equal to zero, then the plane g coincides with the plane of the object's trajectory. The space angles ψ, θ and φ can be expanded by angular velocities Ω_ψ, Ω_θ and Ω_φ, and T_p to the expressions $\tilde{\psi} = \psi + \Omega_\psi T_p$, $\tilde{\theta} = \theta + \Omega_\theta T_p$, and $\tilde{\varphi} = \varphi + \Omega_\varphi T_p$, and exploited to model an induced rotational motion of the object on yaw pitch and role directions.

3. MODEL OF ISAR SIGNAL DETERMINISTIC COMPONENTS

Assume that the ISAR transmits a sequence of N linear frequency modulated pulses each of which is described by the expression

(9) $$\dot{S}(t) = \mathbf{rect}\frac{t}{T}\mathbf{exp}\left\{-j\left[\omega t + bt^2\right]\right\}$$

where $\omega = 2\pi\frac{c}{\lambda}$ is the carrier angular frequency, $c = 3.10^8$ m/s is the speed of the light, λ is the carrier wavelength of the LFM pulse, $b = \frac{2\pi\Delta F}{T}$ is the LFM rate, t is the current time (fast time). T is the time duration of the LFM pulse, ΔF is the bandwidth of the transmitted pulse that provides for the range dimension of the resolution cell, i.e. $\Delta R = c / 2\Delta F$.

The deterministic component of the ISAR signal, reflected by the ijkth point scatterer of the object can be calculated by the expression

(10) $$\dot{S}_{ijk}(p,t) = a_{ijk}\mathbf{rect}\frac{t - t_{ijk}(p)}{T}\mathbf{exp}\left\{-j\begin{bmatrix}\omega\left(t - t_{ijk}(p)\right) + \\ + b\left(t - t_{ijk}(p)\right)^2\end{bmatrix}\right\},$$

where

$$\mathbf{rect}\frac{t-t_{ijk}(p)}{T}=\begin{cases}1,0\le\dfrac{t-t_{ijk}(p)}{T}<1,\\ 0,\dfrac{t-t_{ijk}(p)}{T}<0\\ 0,\dfrac{t-t_{ijk}(p)}{T}\ge 1\end{cases},$$

where a_{ijk} is the reflection coefficient of the ijkth point scatterer of the object, the three dimensional image function; $t_{ijk}(p)=\dfrac{2R_{ijk}(p)}{c}$ is the time delay of the signal reflected by the ijkth point scatterer; $R_{ijk}(p)$ is the modulus of the distance vector to the ijkth point scatterer; t is the time dwell of the ISAR signal, the fast time which in discrete form for the received signal can be written as $t=[k_{ijk\min}(p)+k]\Delta T$, where $k=\overline{0,[k_{ijk\max}(p)-k_{ijk\min}(p)]+K-1}$ is the number of the range bin where a sample of a the LFM pulse is placed; $K=\dfrac{T}{\Delta T}$ is the full number of the samples of the LFM pulse, ΔT is the time duration of a the LFM sample, $k_{ijk\min}(p)=\left\lceil\dfrac{t_{ijk\min}(p)}{\Delta T}\right\rceil$ is the number of the radar range bin where the signal, reflected from the nearest point scatterer of the object is detected, $t_{ijk\min}(p)=\dfrac{2R_{ijk\min}(p)}{2}$ is the minimal time delay of the ISAR signal reflected from the nearest point scatterer of the object, $K(p)=k_{ijk\max}(p)-k_{ijk\min}(p)$ is the relative time dimension of the object measured on the line of sight; $k_{ijk\max}(p)=\left\lceil\dfrac{t_{ijk\max}(p)}{\Delta T}\right\rceil$; is the number of the radar range bin where the signal, reflected from the farthest point scatterer of the object is detected; $t_{ijk\max}(p)=\dfrac{2R_{ijk\max}(p)}{2}$ is the maximum time delay of the ISAR signal reflected from the farthest point scatterer of the object; $R_{ijk}(p)$ is the modulus of the range distance vector to the ijkth point scatterer of the object expressed as

$$R_{ijk}(p)=\left[x_{ijk}^2(p)+y_{ijk}^2(p)+z_{ijk}^2(p)\right]^{\frac{1}{2}}, \tag{11}$$

The current coordinates of the ijk point scatterer can be computed by the following matrix equation

$$\begin{bmatrix}x_{ijk}(p)\\ y_{ijk}(p)\\ z_{ijk}(p)\end{bmatrix}=\begin{bmatrix}x_{00}(0)+V_xT_p\left(\dfrac{N}{2}-1\right)\\ y_{00}(0)+V_yT_p\left(\dfrac{N}{2}-1\right)\\ z_{00}(0)+V_zT_p\left(\dfrac{N}{2}-1\right)\end{bmatrix}+\begin{bmatrix}a_{11}&a_{12}&a_{13}\\ a_{21}&a_{22}&a_{23}\\ a_{31}&a_{32}&a_{33}\end{bmatrix}\begin{bmatrix}X_{ijk}\\ Y_{ijk}\\ Z_{ijk}\end{bmatrix}, \tag{12}$$

where $V_x=V\cos\alpha$ and $V_y=V\cos\beta$ $V_y=V\cos\delta$ are the coordinates of the vector velocity.

The deterministic component of the ISAR signal return is an assembly of signals reflected from all visible

point scatterers placed on the object, i.e.

$$\begin{aligned}\dot{S}(p,t) &= \sum_{ijk}\dot{S}_{ijk}(p,t)\\ &= \sum_{ijk} a_{ijk}\,\mathbf{rect}\,\frac{t-t_{ijk}(p)}{T}\,\mathbf{exp}\left\{-j\left[\begin{array}{l}\omega\left(t-t_{ijk}(p)\right)+\\ +b\left(t-t_{ijk}(p)\right)^2\end{array}\right]\right\}\end{aligned} \tag{13}$$

which in discrete form can be written as

$$\begin{aligned}\dot{S}(p,k) &= \sum_{ijk}\dot{S}_{ijk}(p,k)\\ &= \sum_{ijk} a_{ijk}\,\mathbf{rect}\,\frac{(k_{ijk\min}(p)+k)\Delta T-t_{ijk}(p)}{T}\,\mathbf{exp}\left\{-j\left[\begin{array}{l}\omega\left((k_{ijk\min}(p)+k)\Delta T\right)-t_{ijk}(p)\right)+\\ +b\left((k_{ijk\min}(p)+k)\Delta T\right)-t_{ijk}(p)\right)^2\end{array}\right]\right\}\end{aligned} \tag{14}$$

where

$$\mathbf{rect}\,\frac{(k_{\min}(p)+k)\Delta T-t_{ijk}(p)}{T}=\begin{cases}1 \text{ if } 0\le\dfrac{(k_{ijk\min}(p)+k)\Delta T-t_{ijk}(p)}{T}<1\\ 0 \text{ if } \dfrac{(k_{ijk\min}(p)+k)\Delta T-t_{ijk}(p)}{T}<0\\ 0 \text{ if } \dfrac{(k_{ijk\min}(p)+k)\Delta T-t_{ijk}(p)}{T}\ge 1\end{cases}. \tag{15}$$

For programming implementation all terms, including image function a_{ijk}, rectangular function $\mathbf{rect}\,\frac{(k_{ijk\min}(p)+k)\Delta T-t_{ijk}(p)}{T}$ and exponential function $\mathbf{exp}\left\{-j\left[\begin{array}{l}\omega\left((k_{ijk\min}(p)+k)\Delta T\right)-t_{ijk}(p)\right)+\\ +b\left((k_{ijk\min}(p)+k)\Delta T\right)-t_{ijk}(p)\right)^2\end{array}\right]\right\}$ are presented as multidimensional matrices, arrays, to which entry-wise product is applied.

ISAR signal formation is illustrated in Fig. 2. Each LFM ISAR signal is presented by seven samples and placed in seven range bins with different number. Signals from nearest, first, second and third point scatterers are summed in the range bin $k_{ijk\min}$. In the next range bin signals from nearest, first, second, third and fourth point scatterers are summed. Finally, the signals from third and fourth point scatterers are summed in the eight range bin.

The demodulation of the ISAR signal return is performed by multiplication with a complex conjugated emitted signal, i.e.

$$\begin{aligned}\hat{S}(t,p) &= S(t,p)\times\mathbf{rect}\,\frac{t}{T}\exp\left[-j(\omega t+bt^2\right]=\\ &\sum_i\sum_j\sum_k a_{ijk}\,\mathbf{rect}\,\frac{t-t_{ijk}(p)}{T}\exp\left\{j\left[\omega\left(t-t_{ijk}(p)\right)+b.\left(t-t_{ijk}(p)\right)^2\right]\right\}\times\exp\left[-j(\omega t+bt^2\right]\end{aligned} \tag{16}$$

which yields

$$\hat{S}(t,p)=\sum_i\sum_j\sum_k a_{ijk}\,\mathbf{rect}\,\frac{t-t_{ijk}(p)}{T}\exp\left\{-j\left[(\omega+2bt)t_{ijk}(p)-bt_{ijk}^2(p)\right]\right\}. \tag{17}$$

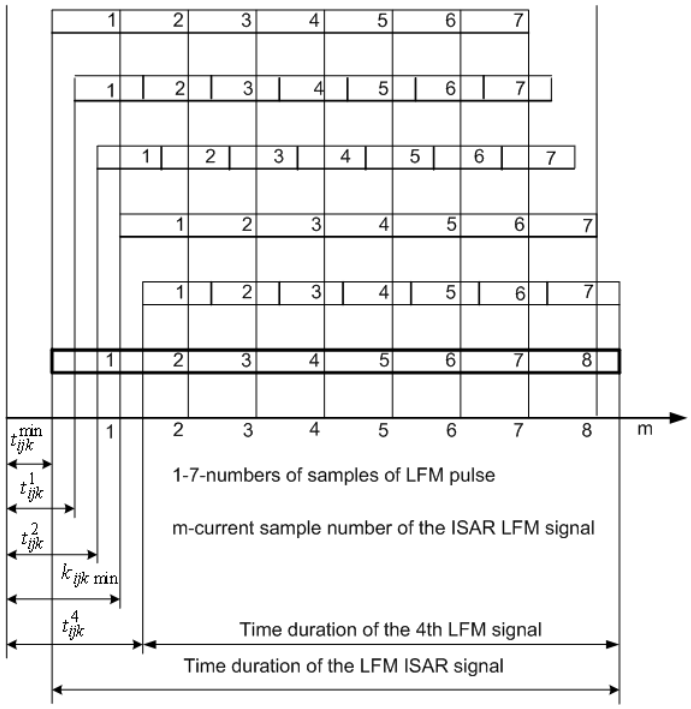

Figure 2: ISAR signal formation

Denote the current angular frequency of emitted LFM pulse as $\omega(t) = \omega + 2bt$, where ω is the carrier angular frequency, and b is the chirp rate. In general case the discrete time parameter can be written as $t = k\Delta T$, where k is the sample number, ΔT is time duration of the sample. The current discrete frequency can be expressed by $\omega_k = k\left(\frac{\omega}{k} + 2b(\Delta T)\right) = k\Delta\omega_k$. Then (17) can be rewritten as

$$(18) \qquad \hat{S}(t,p) = \sum_k \sum_j \sum_i a_{ijk}\,\mathbf{rect}\frac{t - t_{ijk}}{T}\exp\left[-j\left(2\omega(t)\frac{R_{ijk}(p)}{c} - b\left(\frac{2R_{ijk}(p)}{c}\right)^2\right)\right],$$

which in discrete form is

$$(19) \qquad \hat{S}(k,p) = \sum_k \sum_j \sum_i a_{ijk}\,\mathbf{rect}\frac{(k_{\min}(p) + k)\Delta T - t_{ijk}(p)}{T}\exp\left[-j\left(2\omega_k\frac{R_{ijk}(p)}{c} - b\left(\frac{2R_{ijk}(p)}{c}\right)^2\right)\right].$$

The expression (19) can be interpreted as a procedure, that projects the 3-D image function, a_{ijk} onto the 2-D ISAR signal plane, $\hat{S}(k,p)$ by the projective operator, the exponential term

$$(20) \qquad \exp\left[-j\left(2\omega_k\frac{R_{ijk}(p)}{c} - b\left(\frac{2R_{ijk}(p)}{c}\right)^2\right)\right].$$

In this case the image function can be extracted from the ISAR signal plane by the inverse projective operation

$$(21) \qquad a_{ijk} = \sum_p \sum_k \hat{S}(k, p).\exp\left[j\left(2\omega_k \frac{R_{ijk}(p)}{c} - b\left(\frac{2R_{ijk}(p)}{c} \right)^2 \right) \right],$$

where k is the discrete range coordinate measured onto the line of sight, p is the discrete cross range coordinate measured onto the orthogonal direction to the line of sight.
Consequently, the image reconstruction is a procedure of compensation of the phases of all signals reflected from particular point scatterers of the object, induced by the object movement along the line of the inverse synthetic aperture that means to stop the object in a particular place in the space and extract an image.

After coordinate transformation from discrete object coordinates i, j, k to projective coordinates $\hat{k}, \hat{p}$, the argument of the exponential term, $\left(2\omega_k \frac{R_{ijk}(p)}{c} - b\left(\frac{2R_{ijk}(p)}{c} \right)^2 \right)$ can be reduced to the following form

$$(22) \qquad \Phi(k, p) + 2\pi \frac{p\hat{p}}{N} + 2\pi \frac{k\hat{k}}{K},$$

where $\hat{k}, \hat{p}$ are the new coordinates of *ijk*-th point scatterer on a (k, p) plane; $\Phi(k, p)$ is the polynomial of higher order

$$(23) \qquad \Phi(k, p) = a_0(k) + a_1(k).p + a_2(k).p^2 + ... + a_m(k)p^m.$$

The constant term $a_0(k)$ can be assumed zero. The linear term performs linear phase correction (range alignment). The quadratic term performs quadratic phase correction, while the higher order terms perform higher order phase correction.
The substitution of the expression (22) in (21) and reduction of the 3-D image function a_{ijk} into 2-D one, $I(\hat{p}, \hat{k})$ yield

$$(24) \qquad I(\hat{p}, \hat{k}) = \sum_p \sum_k \hat{S}(k, p).\exp\left[j\left(\Phi(k, p) + 2\pi \frac{p\hat{p}}{N} + 2\pi \frac{k\hat{k}}{K} \right) \right]$$

which can be rewritten as

$$(25) \qquad I(\hat{p}, \hat{k}) = \sum_p \left[\sum_k \hat{S}(k, p).\exp\left[j\Phi(k, p) \right] \exp\left(j2\pi \frac{k\hat{k}}{K} \right) \right] \exp\left(j2\pi \frac{p\hat{p}}{N} \right).$$

4. IMAGE RECONSTRUCTION ALGORITHM

The expression (25) can be considered as an image reconstruction procedure, which does reveal the 2-D discrete complex image function $I(\hat{p}, \hat{k})$. The image reconstruction can be implemented by the following computational operations. First, phase correction of the complex matrix $\hat{S}(k, p)$ by multiplication with complex exponential term $\exp\left[j\Phi(k, p) \right]$, i.e.

$$(26) \qquad \tilde{S}(k, p) = \hat{S}(k, p).\exp\left[j\Phi(k, p) \right].$$

Second, range compression by discrete inverse Fourier transform of the phase corrected complex matrix $\tilde{S}(k, p)$ on the range coordinate k, i.e.

$$(27) \qquad \tilde{S}(\hat{k}, p) = \frac{1}{k_{\max}(p) - k_{\min}(p) + K} \sum_{k} \tilde{S}(k, p).\exp\left(j2\pi \frac{k\hat{k}}{K} \right).$$

Third, image extraction by discrete inverse Fourier transformation of a range compressed complex matrix $\tilde{S}(p, \hat{k})$ on the cross range coordinate *p*, i.e.

$$(28) \qquad I(\hat{k}, \hat{p}) = \frac{1}{N} \sum_{p=1}^{N} \tilde{S}(\hat{k}, p).\exp\left(j2\pi \frac{p\hat{p}}{N} \right).$$

The phase correction function $\Phi(k, p)$ is a priory unknown. Therefore, it is impossible to perform the aforementioned image extraction algorithm. Taking into account the linear property of the operations in (25), the image extraction algorithm may start with 2-D discrete Fourier transform (range compression and cross range compression) over the demodulated ISAR signal, the complex matrix $\hat{S}(k, p)$

$$(29) \qquad \hat{I}(\hat{p}, \hat{k}) = \sum_{p=1}^{N} \left[\sum_{k=1}^{K} \hat{S}(k, p).\exp\left(j2\pi \frac{k\hat{k}}{K} \right) \right] \exp\left(j2\pi \frac{p\hat{p}}{N} \right).$$

If the image obtained by the procedure (29) is blurred it is necessary an autofocusing phase correction procedure to be applied, i.e. to perform the operation $\tilde{S}(k, p) = \hat{S}(k, p).\exp\left[j\Phi(k, p) \right]$. It requires defining $\Phi(k, p)$ and calculating the coefficients $a_1(k)\ a_2(k) \ldots\ a_m(k)$ in the polynomial

$$(30) \qquad \Phi(k, p) = a_1(k).p + a_2(k).p^2 + \ldots + a_m(k)p^m \ .$$

It can be implemented iteratively using the entropy as a cost function to evaluate the quality of the ISAR image. The computational load can be reduced if the coefficients $a_m(k)$ are constant, i.e. $a_m(k) = a_m$, and $\Phi(k, p) = \Phi(p)$. The coefficients are defined on stages. On the first stage a_1 is calculated, on the second - a_2 and so on. The exact value of the coefficient a_m is computed iteratively stepwise, starting from $a_m = 0$ and incrementing by step $\Delta a_m = \pm 0.01$ if the image quality gets better. If the image quality does not improve or gets worst go to computation of the next coefficient a_{m+1} or stop the procedure.

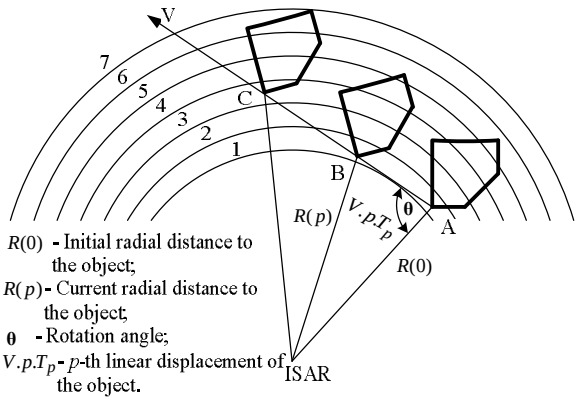

Figure 3: The object travels several range bins during the observation time.

It is worthy to note that the object travels several range bins during the observation time due to the translational motion of the mass center on the line of sight (Fig. 3). The phase correction algorithm puts

each reference point in its initial range bin and compensates for all ISAR signal's phases induced by the motion of high order.

4.1. Phase Correction Based on Entropy Minimization

Let $\Phi_s(p)$ be the phase correction function, defined on the sth step. The autofocusing phase correction is performed by multiplication of the demodulated ISAR signal, matrix $\hat{S}(p,k)$, by the exponential term $\exp(j\Phi_s(p))$, i.e.

(31) $$\tilde{S}_s(p,k) = \hat{S}(p,k)\exp(j\Phi_s(p)).$$

After current phase correction (31) and image extraction by expressions (26), (27) and (28) define the power normalized image as

(32) $$\bar{I}_s(\hat{p},\hat{k}) = \frac{\left|\hat{I}_s(\hat{p},\hat{k})\right|^2}{\sum_{p=0}^{N-1}\sum_{k=0}^{K-1}\left|\hat{I}_s(\hat{p},\hat{k})\right|^2}.$$

Define the entropy as an image cost function of the normalized ISAR image

(33) $$H_s = -\sum_{p=0}^{N-1}\sum_{k=0}^{K-1}\bar{I}_s(\hat{p},\hat{k})\ln[I_s(\hat{p},\hat{k})].$$

The procedure is repeated until the global minimum value of the entropy H_s is acquired. The estimate of the phase correction function corresponds to the minimum of the entropy image cost function, i.e.

(34) $$\hat{\Phi}(p) = \arg\min_{\Phi}\left\{H[\bar{I}_s(\hat{p},\hat{k})]\right\}.$$

5. NUMERICAL EXPERIMENT

To verify the properties of the developed 3-D model of the LFM ISAR signal and to prove the correctness of the image reconstruction procedure including range alignment, range compression, azimuth compression and autofocusing a numerical experiment is carried out. It is assumed that the object detected in 3-D coordinate system $O'XYZ$ is moving rectilinearly in a 3-D Cartesian coordinate system of observation $Oxyz$. Trajectory parameters: the modulus of the vector velocity and coordinate angles $V = 600$ m/s, $\alpha = \frac{5.5}{6}\pi$, $\beta = -\frac{\pi}{2}$, $\gamma = \frac{2.5}{6}\pi$; the mass-center coordinates at the moment $p = N/2$: $x_{00}(0) = 0$ m; $y_{00}(0) = 5.10^4$ m; $z_{00}(0) = 3.10^3$ m, the coordinates of the point $R(0)$ from the reference plane $x_0(0) = 10$ m; $y_0(0) = 5.10^4$ m; $z_0(0) = 2.10^3$ m, the position angle between the reference plane and plane $O'XY$ in the object space $(g\alpha) = \frac{\pi}{2}$. Parameters of the ISAR emitted pulse: the wavelength $\lambda = 3.10^{-2}$ m, the pulse repetition period $T_p = 5.10^{-3}$ s, the time duration of the transmitted LFM pulse $T = 10^{-6}$ s, the number of samples of LFM emitted signal $K = 128$, the carrier frequency $f = 10^{10}$ Hz, the time duration of LFM pulse sample $\Delta T = \frac{T}{K} = 0.78.10^{-8}$ s, the bandwidth of LFM signal $\Delta F = 1.5.10^8$ Hz, the LFM rate $b = 4.71.10^{14}$ [1/s^2], the number of emitted pulses N = 128. The whole geometry of the object is depicted in a 3-D regular rectangular grid. Dimensions of the grid's cell: $\Delta X = \Delta Y = \Delta Z = 0.5$ m.

The number of the reference points on the grid axes $O'X$, $O'Y$ and $O'Z$: $I = 64$, $J = 64$ and $\hat{K} = 10$. The point scatterers are placed in each node of the regular grid: the normalized intensities of the point scatterers placed on the object $a_{ijk} = 0.01$. The computational results of the numerical experiment are presented in Figs 4 and 5. The unfocused image obtained by first application of 2-D FFT to the matrix $\hat{S}(p,k)$ and the normalized unfocused image are given in Fig. 4, *a*, and Fig. 4, *b*, respectively.

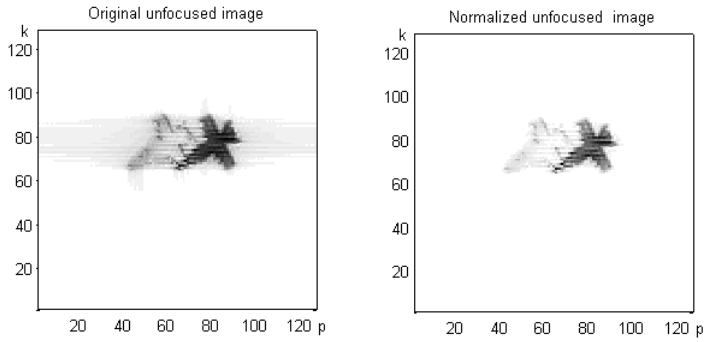

Figure 4: Unfocused image obtained by first application of 2-D FFT to the ISAR signal, matrix $\hat{S}(p,k)$: original unfocused image (*a*), normalized unfocused image (*b*)

The final focused image obtained by application of the phase correction procedure to the matrix $\hat{S}(p,k)$ is presented in Fig. 5, *a*. The evolution of the entropy image function with minimum value 6.1961, obtained on the 47th iteration is illustrated in Fig. 5, b. The evolution of the entropy image function after 47th iteration where the procedure has to be stopped is presented in Fig. 5, *c*.

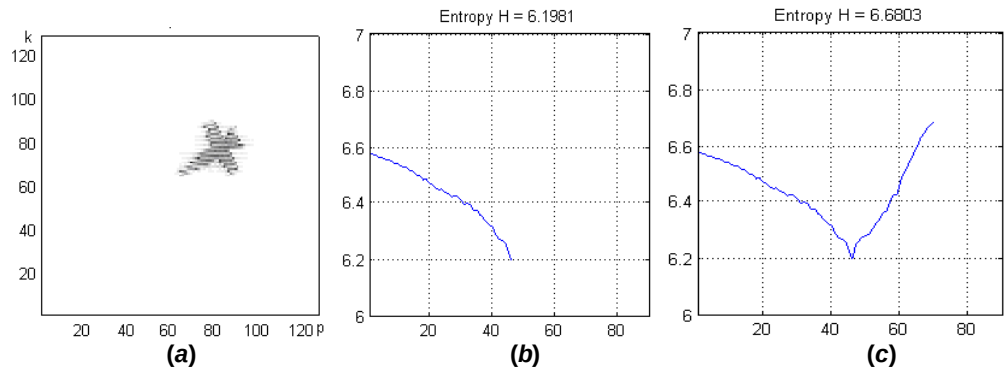

Figure 5: Ultimate focused image obtained by application of the phase correction procedure to the ISAR signal, matrix $\hat{S}(p,k)$ (*a*), and evolution of the entropy image function with minimum value 6.1961, obtained on 47th iteration (*b, c*).

6. CONCLUSION

In the present work a new model of the LFM ISAR signal has been developed. The model describes the amplitude and phase distribution of ISAR signals reflected from the surface of a object with a complicated shape. The geometry of the object has been depicted by reference points in 3-D coordinate system. Basic analytical geometrical and kinematical equations have been derived. The model allows describing variety of kinematical states of the object. A mathematical model of the deterministic component of the ISAR signal return, presented as a geometrical sum of the emissions of the point sctterers from the object space has been derived. For each emitted pulse the model represents the profile of the ISAR signal return along the range direction**.** A new mathematical definition of the discrete fast time parameter as a function of the

number of radar range resolution cells has been suggested. Description and graph illustration of the process of the LFM ISAR signal formation has been presented. All stages of image reconstruction, including demodulation, range alignment, range compression, azimuth compression and autofocusing have been mathematically described. Entropy function has been used to implement iterative image quality enhancement. Numerical experiment to verify the ISAR geometry and ISAR signal model, and image reconstruction algorithms has been carried out.

REFERENCES

[1] Boultadakis, G., K. Skrapas, P. Frangos. Time – frequency analysis of radar signals, RTO / SET 080 Int. Sym. on 'Target Identification and Recognition Using RF Systems, Oslo, Norway, 2004.

[2] Chen, V. C., S. Qian. Joint time-frequency transform for radar range-Doppler Imaging, IEEE Transactions on Aerospace and Electronic Systems, AES-34, 2, 1998, pp. 486-499.

[3] Qian, S., V. C. Chen, 1998, ISAR motion compensation via adaptive joint time-frequency technique, IEEE Transactions on Aerospace and Electronic Systems, AES-34, 2, 1998, pp. 670-677.

[4] Palmer, J., J. Homer, I. D. Longstaff, M. Martorella, B. Littleton. ISAR imaging using an emulated multistatic radar system, IEEE, Transaction on AES, vol. 41, 4, 2005, pp 1464-1471.

[5] Itoh, T.H., Sueda, Y. Watanabe. Motion compensation for ISAR via centroid tracking, IEEE, Transaction on Aerospace and Electronic Systems, vol.AES-32, No 1, 1996, pp. 1191-1197.

[6] D.E. Wahl, P.H. Eichel, D.C. Ghiglla, and C. V. Jakowatz, Phase gradient autofocus - A robust tool for high resolution SAR phase correction, IEEE Transactions on Aerospace and Electronic Systems, vol. AES-30, No 3 (1994) 827-835.

[7] S. W. Werness, Carrara, L. Joyce, and D. Franczak "Moving target imaging algorithm for SAR data, IEEE Transactions on Aerospace and Electronic Systems, vol. AES-26, No 1, 1990, pp. 57-67.

[8] Martorella, M., F. Berizzi. Time windowing for highly focused ISAR image reconstruction, IEEE Transaction on AES vol. 41, 3, 2005, pp 992-1007.

[9] Xi, L., L. Guosui, J. Ni. Autofocusing of ISAR images based on entropy minimization, IEEE Transactions on Aerospace and Electronic Systems, AES-35, 4, 1999, pp. 1240-1252.

[10] Li J., R. Wu, V. Chen. Robust autofocus algorithm for ISAR imaging of moving targets, IEEE Transactions on Aerospace and Electronic Systems, AES-37, 3, 2001, pp. 1056-1069.

[11] Jiang N., R.Wu, J Li, "Super resolution feature extraction of moving targets," IEEE Transactions on Aerospace and Electronic Systems, vol. AES-37, No 3, pp. 781-793, 2001.

[12] Berizzi, F., G. Cosini. Autofocusing of inverse synthetic aperture radar images using contrast optimization. IEEE Transactions on Aerospace and Electronic Systems, 32, 3, 1996, pp 1185-1191.

[13] Liu G., J. Li, "Moving target detection via airborne HRR phased array radar," IEEE Transactions on Aerospace and Electronic Systems, vol. AES-37, No 3, pp 914-924, 2001.

[14] Bi, Zh., Li J., Liu, Z-S, "Super resolution SAR imaging via parametric spectral estimation methods," IEEE Transactions on Aerospace and Electronic Systems, AES-35, 1, 1999, pp. 267-281.

[15] Wu, R., Li J., Z-S Liu, "Super resolution time delay estimation via MODE-WRELAX," IEEE Transactions on Aerospace and Electronic Systems, AES-35, 1, 1999, pp. 294-307.

[16] Wang, G., Xiang-Gen, Xia, Victor Chen. Three-dimensional ISAR imaging of maneuvering targets using three receivers, IEEE Transactions on Image Processing, IP-10, 3, 2001, pp. 436-446.

[17] Stuff M.A. "Three dimensional analysis of moving target radar signals," Methods and implications for ATR and feature aided tracking. Proceeding of SPIE, 3721 (Algorithms for SAR imagery VI), 1999, pp 485-496.

[18] Mayhan J.T., M.L.Burrows, K.M. Cuomo, "High resolution 3D "Snapshot" ISAR imaging and feature extraction," IEEE Transactions on Aerospace and Electronic Systems, vol. AES-37, 2001, pp 630-642.

[19] Garvanov, and C. Kabakchiev, "Average Decision Threshold of CA CFAR and Excision CFAR Detectors in the Presence of Strong Pulse Jamming", German Radar Symposium, Bonn, Germany, September, 2002, pp. 615-620.